UNSTEADY TRANSONIC FLOW

USING EULER EQUATIONS

Dave M. Belk
L. Bruce Simpson
Air Force Armament Laboratory
Eglin Air Force Base, Florida

Outline

An implicit, two-factor, split flux, finite volume Euler equations solution algorithm is applied to the time-accurate solution of transonic flow about an NACA0012 airfoil and a rectangular planform supercritical wing undergoing pitch oscillations. Accuracy for Courant numbers greater than one is analyzed. Freezing the flux Jacobians can result in significant savings for steady-state solutions; the accuracy of freezing flux Jacobians for unsteady results is investigated. The Euler algorithm results are compared with experimental results for an NACA 0012 and a rectangular planform supercritical wing (Figure 1).

- ALGORITHM
- TIME ACCURACY FOR COURANT NUMBERS GREATER THAN ONE
- FREEZING FLUX JACOBIANS
- COMPARISON WITH EXPERIMENT
  - NACA0012
  - RECTANGULAR SUPERCRITICAL WING

Figure 1

Three Dimensional Euler Equations

The Euler equations model inviscid flow with entropy and vorticity being generated by shocks. Many unsteady flows of practical interest require that viscous effects be included. One advantage of the Euler equations solution algorithm is that it is easily extended to include viscous effects.

The three-dimensional time-dependent Euler equations in conservation form are written in a general time-dependent boundary conforming curvilinear coordinate system. This time-dependent coordinate transformation provides for a dynamic grid that can follow the motion of the body (Figure 2). The details of this transformation are given in Reference 1.

$$\frac{\partial q}{\partial t} + \frac{\partial f}{\partial x} + \frac{\partial g}{\partial y} + \frac{\partial h}{\partial z} = 0$$

where

$$q = \left[\rho,\ \rho u,\ \rho v,\ \rho w,\ e\right]^T$$

TIME DEPENDENT COORDINATE TRANSFORMATION

$$\xi = \xi(x,y,z,t) \qquad \tau = \tau(t)$$

$$\eta = \eta(x,y,z,t)$$

$$\zeta = \zeta(x,y,z,t)$$

$$\frac{\partial Q}{\partial \tau} + \frac{\partial F}{\partial \xi} + \frac{\partial G}{\partial \eta} + \frac{\partial H}{\partial \zeta} = 0$$

Figure 2

Algorithm

An implicit split flux finite volume solution algorithm for the Euler equations is obtained. Flux Jacobians with superscript L correspond to information propagating in the positive curvilinear coordinate direction, and flux Jacobians with superscript R correspond to information propagating in the negative curvilinear coordinate direction. The equation is then factored into two factors as discussed by Whitfield in Reference 2. The first equation of the two-pass scheme requires the solution of a sparse lower block triangular system by a simple forward substitution, while the second equation requires the solution of a sparse upper block triangular system by a simple backward substitution.

This algorithm is first-order accurate in time and second order accurate in space. A simple modification to use three point backward time differencing will result in second order time-accuracy (Figure 3).

- FINITE VOLUME
- FLUX SPLIT
- IMPLICIT

$$[\ I + \Delta\tau(\ \delta\xi^i A^{L\cdot} + \delta\xi^i A^{R\cdot} + \delta\eta^i B^{L\cdot} + \delta\eta^i B^{R\cdot} + \delta\zeta^i C^{L\cdot} + \delta\zeta^i C^{R\cdot})\ ]\ \Delta Q^n = -\Delta\tau R^n$$

WHERE

$$R^n \equiv \delta\xi^e F^n + \delta\eta^e G^n + \delta\zeta^e H^n$$

- TWO-PASS

$$[\ I + \Delta\tau(\ \delta\xi^i A^{L\cdot} + \delta\eta^i B^{L\cdot} + \delta\zeta^i C^{L\cdot})\ ]\ X^n = -\Delta\tau R^n$$

$$[\ I + \Delta\tau(\ \delta\xi^i A^{R\cdot} + \delta\eta^i B^{R\cdot} + \delta\zeta^i C^{R\cdot})\ ]\ \Delta Q^n = X^n$$

Figure 3

NACA0012 221 x 20 'C' Grid

All of the Euler computations for the NACA0012 airfoil used the 221 x 20 'C' algebraic grid shown below. The grid was generated using Joe Thompson's grid generation code (Reference 3). See Figure 4.

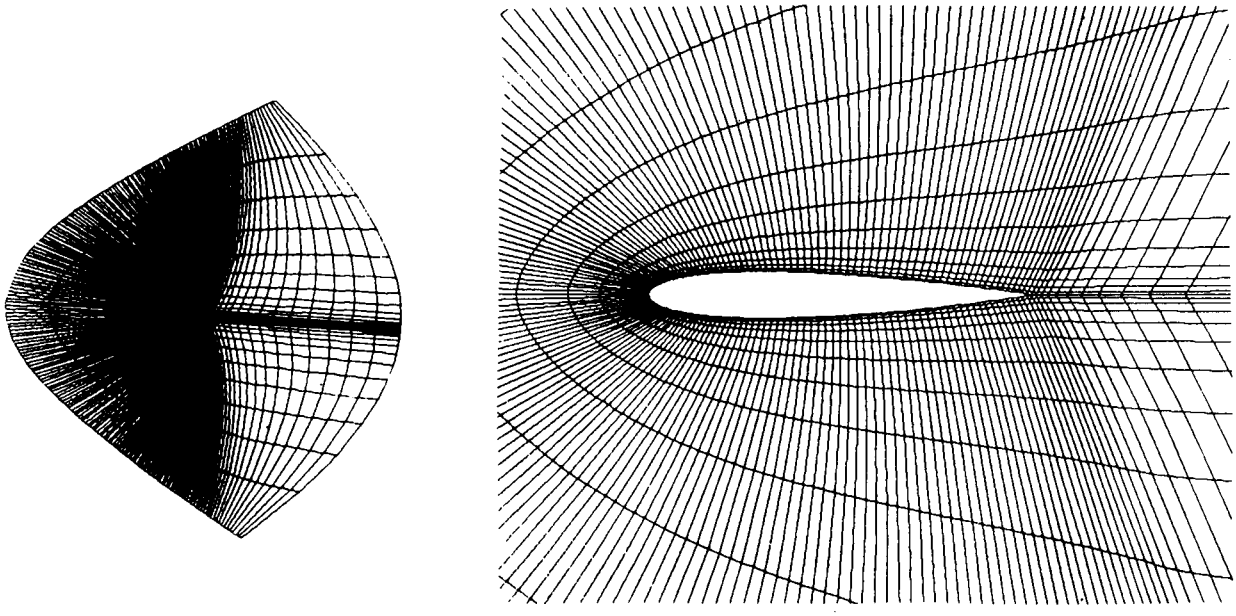

NACA0012 221 x 20 'C' Grid

Figure 4

NACA0012 Lift Coefficients

Calculations were made for a NACA0012 airfoil at Mach = 0.755 oscillating in pitch about the 1/4 chord point with a reduced frequency of k = (ωc/V) = 0.1628. The airfoil had a mean angle of attack = 0.016 degrees and an unsteady alpha = 2.51 degrees. Steady state solutions were obtained at the mean conditions prior to an abrupt start of the oscillatory motion. The calculations were performed for four complete cycles of motion. The figure below shows lift coefficient vs time for three different time step sizes. DTMIN = 0.01 gave 5000 time steps per cycle of motion and corresponds to a maximum Courant number of 10. DTMIN = 0.10 was 500 time steps per cycle of motion and corresponds to a maximum Courant number of 100. DTMIN = 0.20 was 250 time steps per cycle of motion and corresponds to a maximum Courant number of 200. Lift coefficients were only slightly different for the various time step sizes (Figure 5).

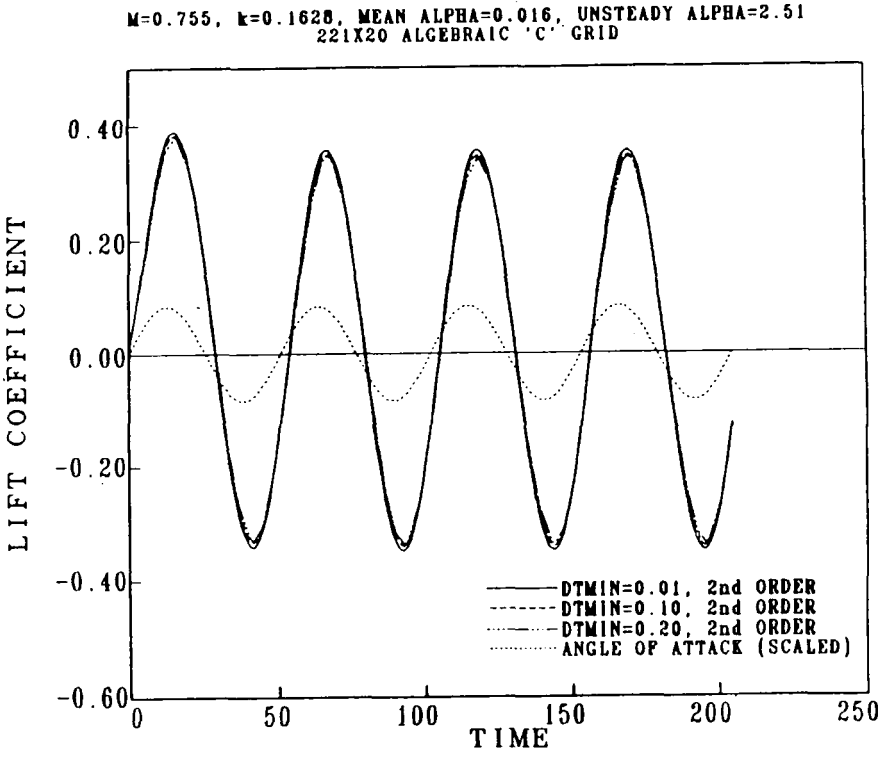

Figure 5

NACA0012 Unsteady Pressure Distributions
340° of Oscillatory Motion

After 340° of oscillatory motion, the angle of attack is increasing through -0.84 degrees. A shock has formed on the lower surface near the 44% chord location. At this point in the motion, the shock is nearly stationary and of maximum strength. The figure below shows the coefficient of pressure distribution along the airfoil. Calculations were done using both first and second order time-accurate differencing and various time step sizes. The results show that all the methods are nearly equivalent for this case (Figure 6).

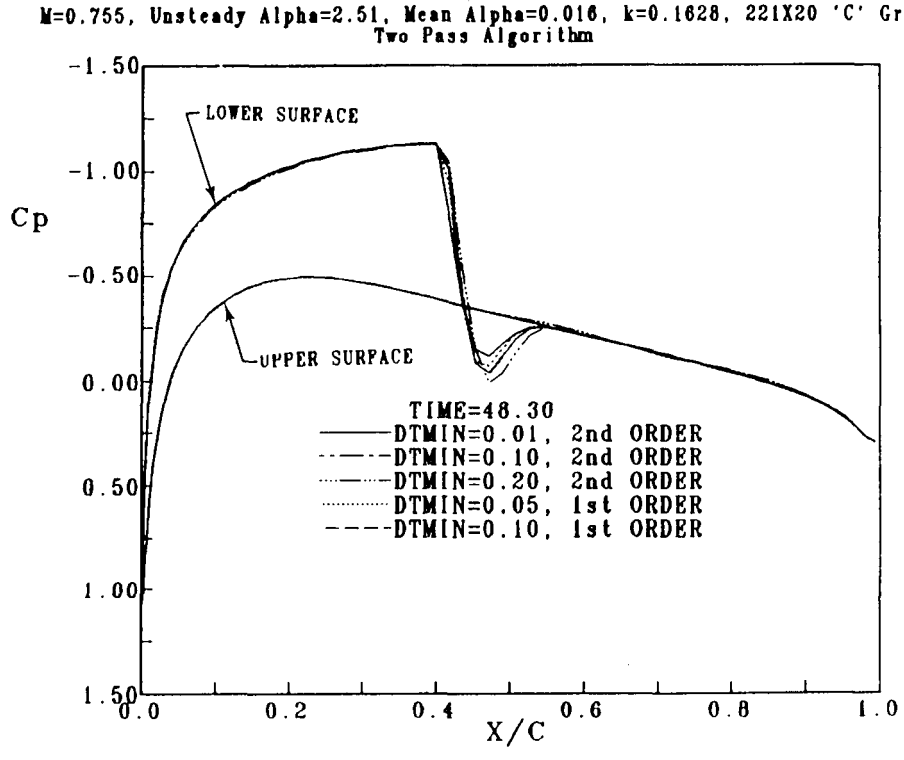

340° OF OSCILLATORY MOTION, INCREASING THROUGH -0.84°

Figure 6

NACA0012 Unsteady Pressure Distributions
25° of Oscillatory Motion

Shortly after the next cycle of motion begins, the shock on the lower surface starts to collapse and move forward. As the angle of attack increases through 1.09°, the shock speed becomes maximum. The figure below shows coefficient of pressure along the airfoil for first and second order differencing and the same time step sizes as in Figure 5. Very little difference is observed between first and second order solutions, but considerable difference in the shock location is noted for different time step sizes. However, as noted previously, the difference in lift coefficient is relatively small (Figure 7).

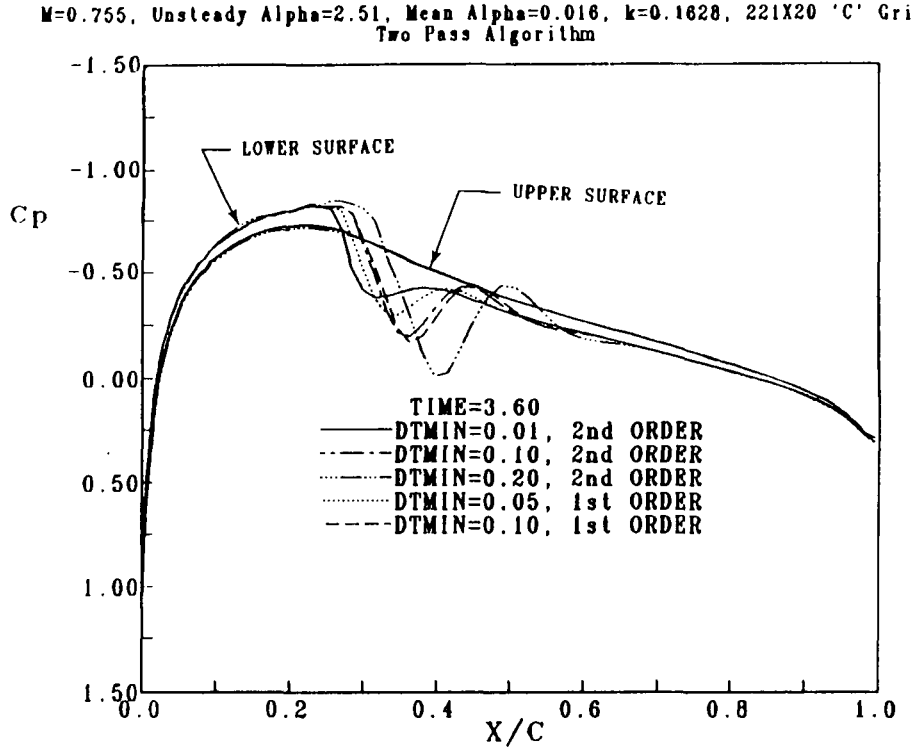

25° OF OSCILLATORY MOTION, INCREASING THROUGH 1.09°

Figure 7

Shock Location

Defining the shock location as the axial location where the pressure coefficient equals the critical pressure (for Mach = 0.755, $C_p^* = -0.5143$), the figure below shows shock location given at different time step sizes. The figure shows that the shock location appears asymptotic to a value as the time step decreases. This indicates that reduction of the time step size below 0.01 should not be expected to change the shock location appreciably (Figure 8).

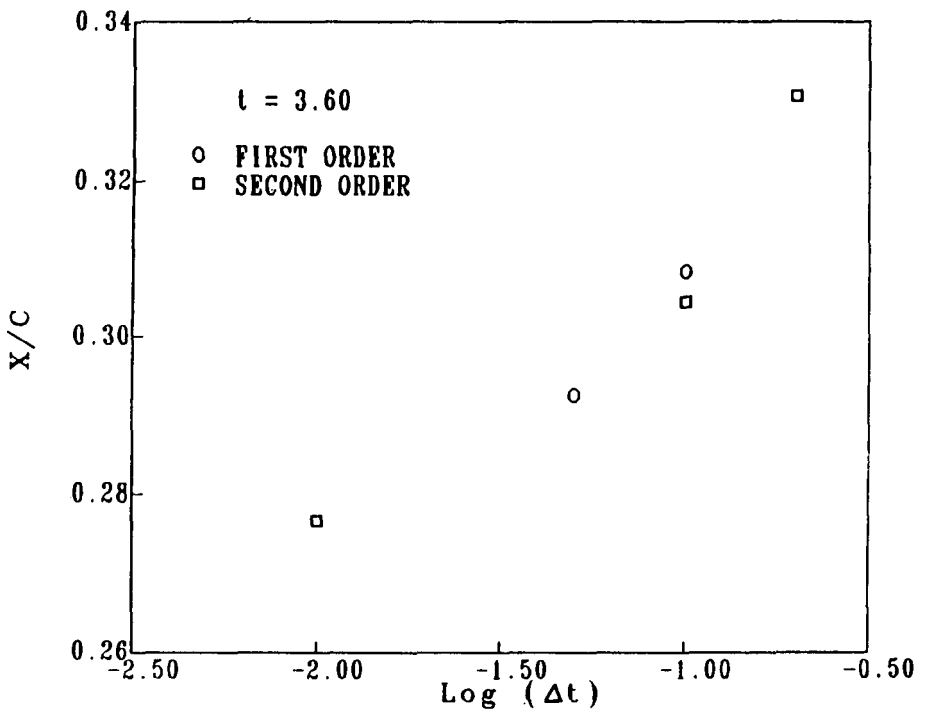

SHOCK LOCATIONS GIVEN BY DIFFERENT TIME STEP SIZES

Figure 8

Freezing the Flux Jacobians for Steady State Conditions

The implicit equations to be solved have the flux Jacobians as coefficients. Since the flux Jacobians, A^L, A^R, B^L, etc., are functions of the current values of Q, they should be updated at each time step. However, D. L. Whitfield has shown steady calculations in which he did not update (froze) the Jacobians and at convergence obtained identical results with calculations updating the Jacobians each time step. The table below shows the obvious computational savings by not doing the extra calculations each time step (Figure 9).

$$A^L = \frac{\partial F^L(Q)}{\partial Q}, \quad A^R = \frac{\partial F^R(Q)}{\partial Q}, \quad B^L = \frac{\partial G^L(Q)}{\partial Q}, \quad \cdots$$

	CYCLES	CPU SEC	MWD	RESID	$\frac{\text{CPU SEC}}{\text{POINT}\cdot\text{CYCLE}}$
IMPLICIT UPDATING JACOBIANS	250	3492	3.26	10^{-4}	$7.8\cdot10^{-5}$
IMPLICIT FREEZING JACOBIANS	250	1527	3.26	10^{-4}	$3.4\cdot10^{-5}$

(8 BLOCK FINNED BODY CALCULATION)

Figure 9

Freezing the Flux Jacobians for Unsteady Calculations

The effect of freezing the Jacobians for unsteady calculations were studied using the oscillatory NACA0012 as the test case. The conditions tested were the same as previously shown. The table below again shows the obvious savings from updating every 10th step (which equates to 3.6° of oscillatory motion) and for never updating the Jacobians. The case listed as never updated used Jacobians from the steady state condition just prior to start of motion. Other cases tried were Jacobians from the freestream starting conditions, updating every 25th step and updating every 50th step. Each of these resulted in stability problems (Figure 10).

JACOBIAN UPDATE FREQUENCY	STEPS	CPU SEC	CPU SEC / POINT STEPS	PERCENT
EVERY STEP	4510	1716	8.61×10^{-5}	100%
EVERY 10TH STEP	5400	1382	5.79×10^{-5}	67%
NEVER UPDATED	5400	1311	5.49×10^{-5}	64%

NACA0012 PITCHING ABOUT 1/4 CHORD

Figure 10

Effect of Frozen Jacobians on Lift Coefficient

Lift coefficient vs time for each of the two frozen Jacobian cases which proved to be stable are compared with the solution from updating every time step. All three solutions used 1st order time-accurate algorithm and a time step size of 0.05. One cannot discern a difference in the three curves shown below (Figure 11).

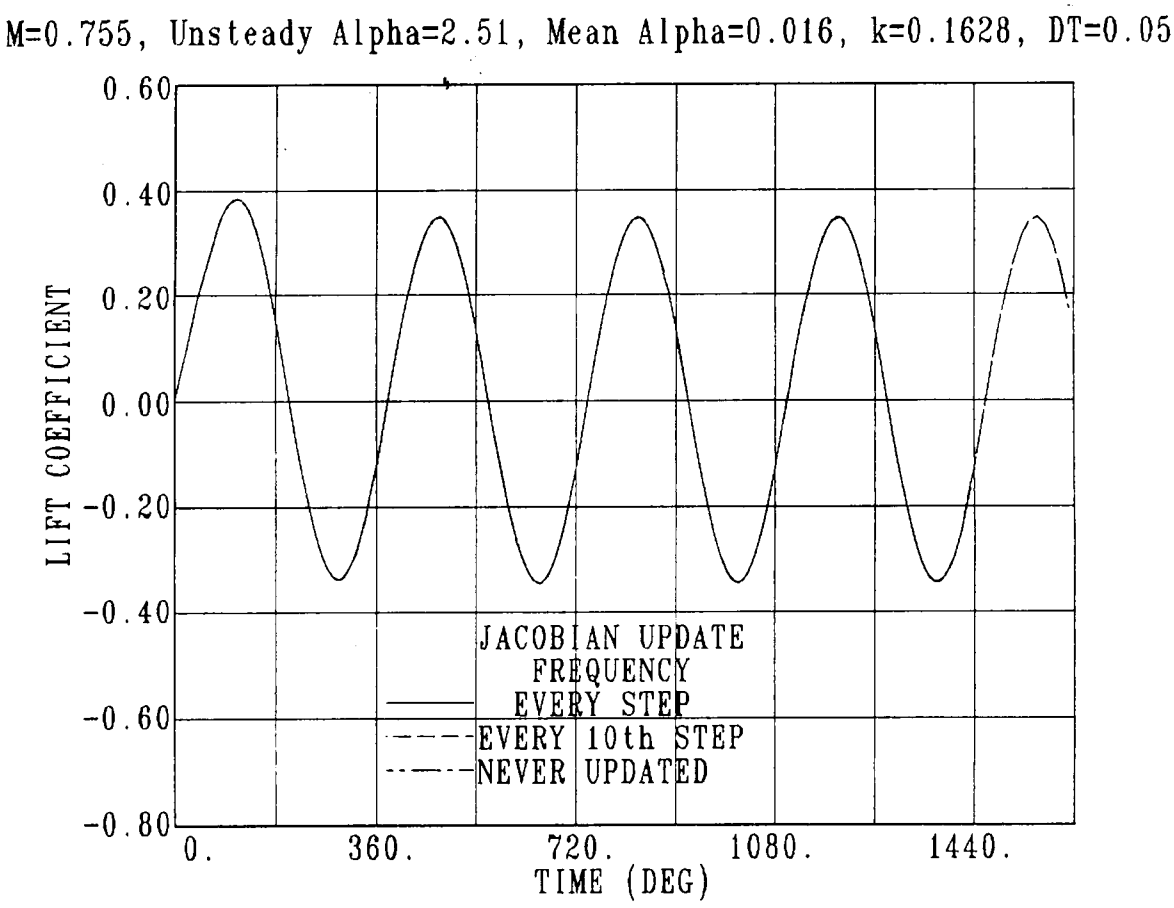

Figure 11

NACA0012 Unsteady Pressure Distributions
25 Degrees

A plot of pressure coefficient along the body for the three cases at 25 degrees of oscillatory motion is shown below in Figure 12. This is the same flow condition described earlier, when the angle of attack is increasing through 1.09 degrees and the shock speed is near a maximum as the shock on the lower surface collapses. Very little difference is noted in the three curves with the only perceivable difference being in the shock location similar to the results shown in Figure 7.

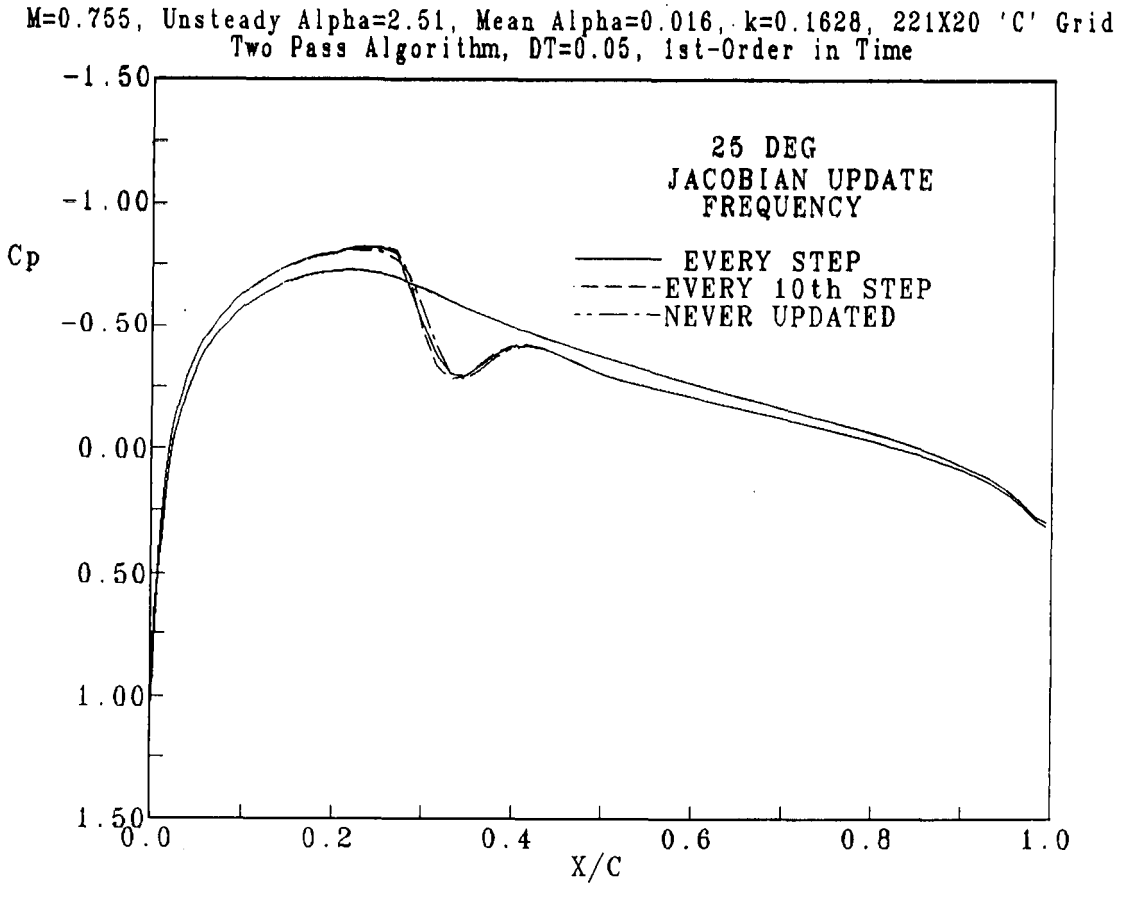

Figure 12

NACA0012 Unsteady Pressure Distributions
70 Degrees

A plot of pressure coefficient along the body for the three cases at 70 degrees of oscillatory motion is shown below. This condition is when angle of attack is increasing through 2.37 degrees and the shock on the upper surface is strengthening and moving downstream. Again, the three solutions are identical except at the shock location. Note that the never updated Jacobian shows a slight ringing action near the shock (Figure 13).

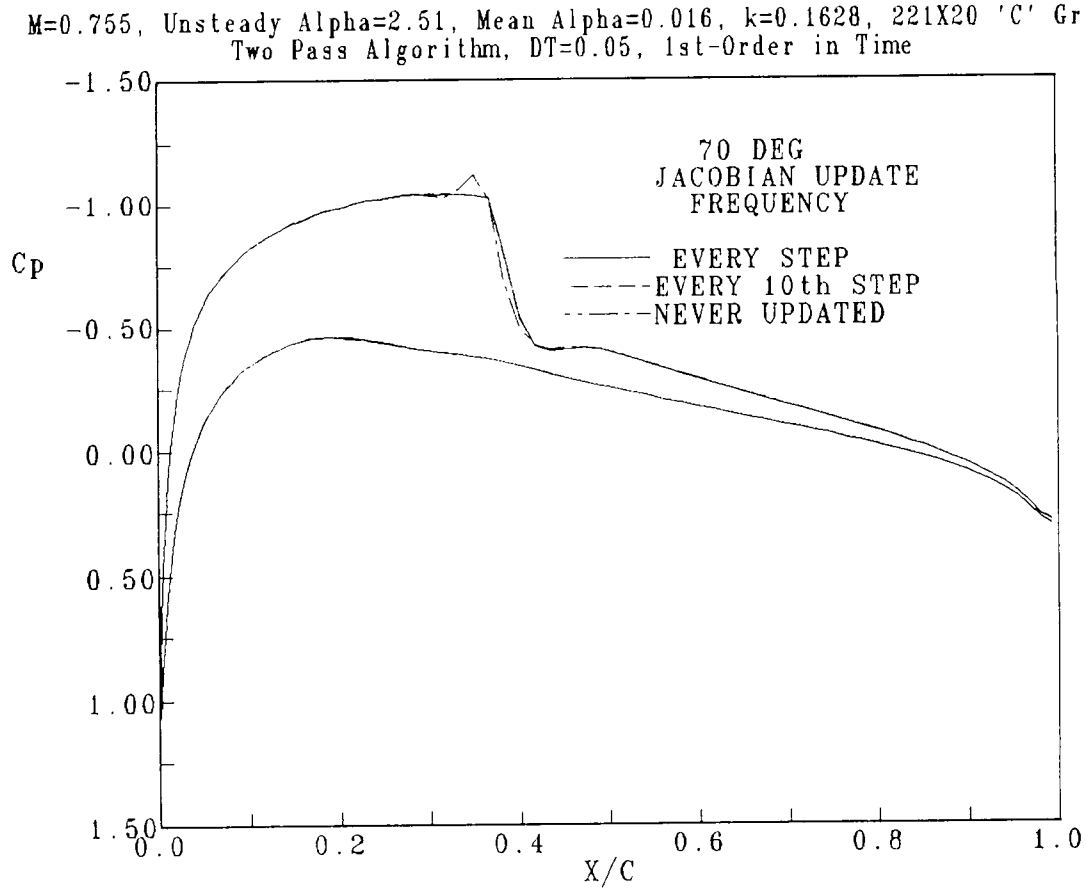

Figure 13

NACA0012 Lift Coefficients

A comparison of calculated lift coefficients with the experimental results of Landon (Reference 4) is given in Figure 14. The experimental results were given for one cycle of motion and are duplicated through four cycles on the figure to compare to the calculations. Examination of experimental lift coefficient reveals a bias towards positive lift not consistent with the small mean angle of attack reported for the symmetric airfoil. A correction to the mean angle of attack was calculated to account for this bias. The following figures show calculations using both the nominal angle of attack of 0.016 degrees and the 'corrected' angle of attack of 0.375 degrees. The freestream Mach is 0.755, reduced frequency is 0.1628, and the unsteady angle of attack amplitude is 2.51 degrees.

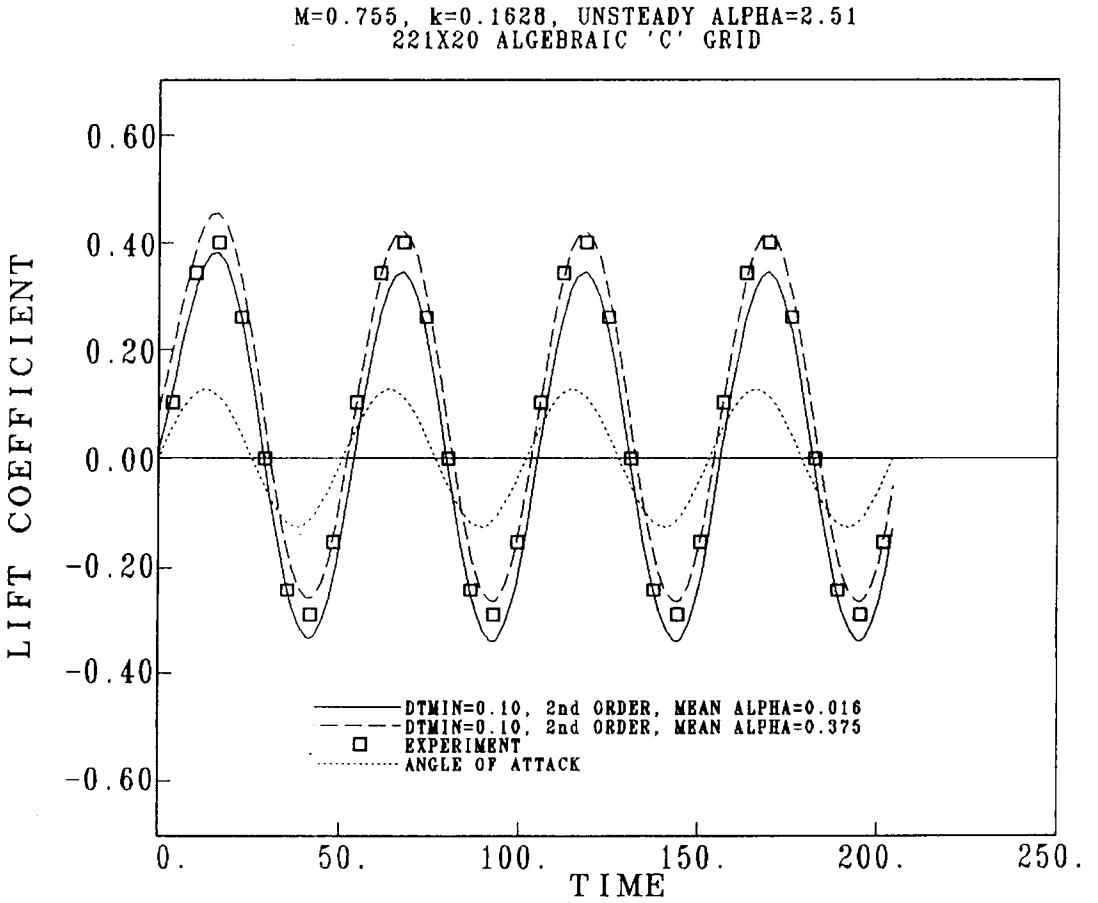

Figure 14

NACA0012 Moment Coefficients

Moment coefficients do not compare with experiment as well as lift, particularly for the negative moments. The 'corrected' mean alpha of 0.375 did not improve the comparison (Figure 15).

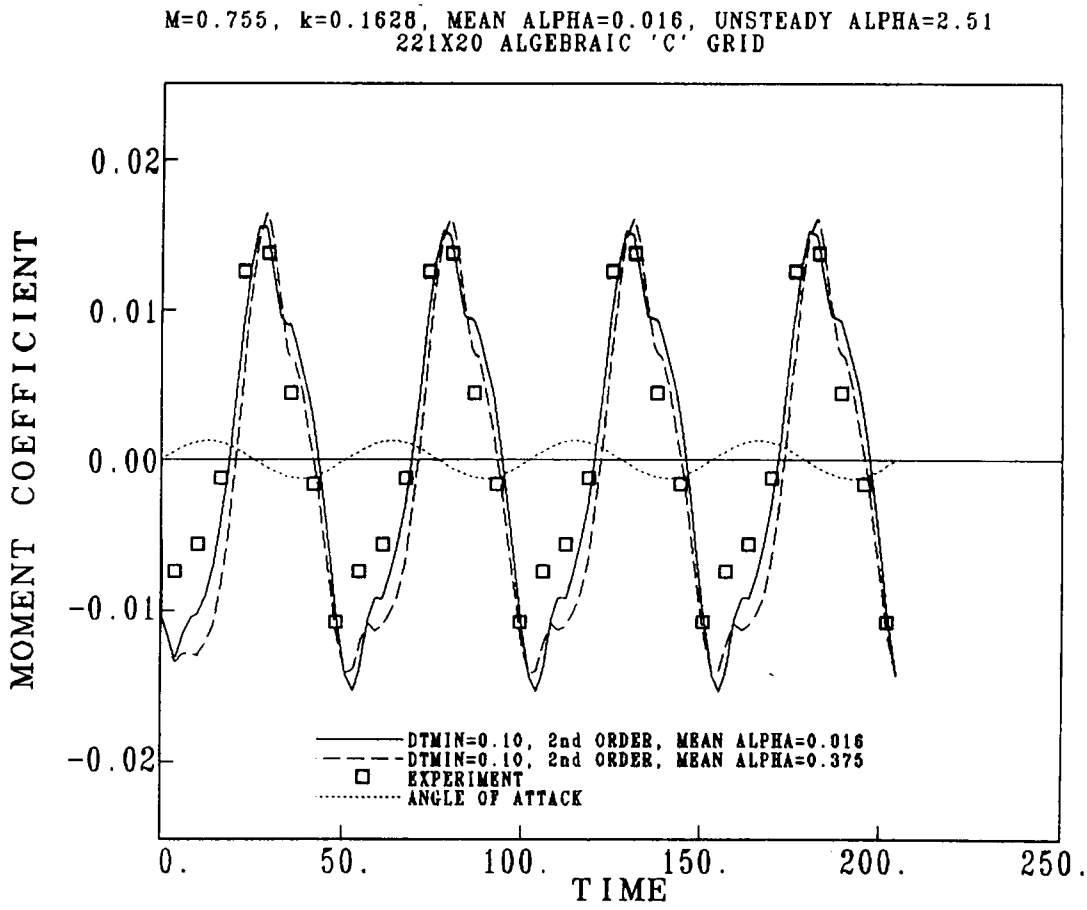

Figure 15

The comparison of calculated and experimental pressure distributions is shown in Figures 16 through 21.

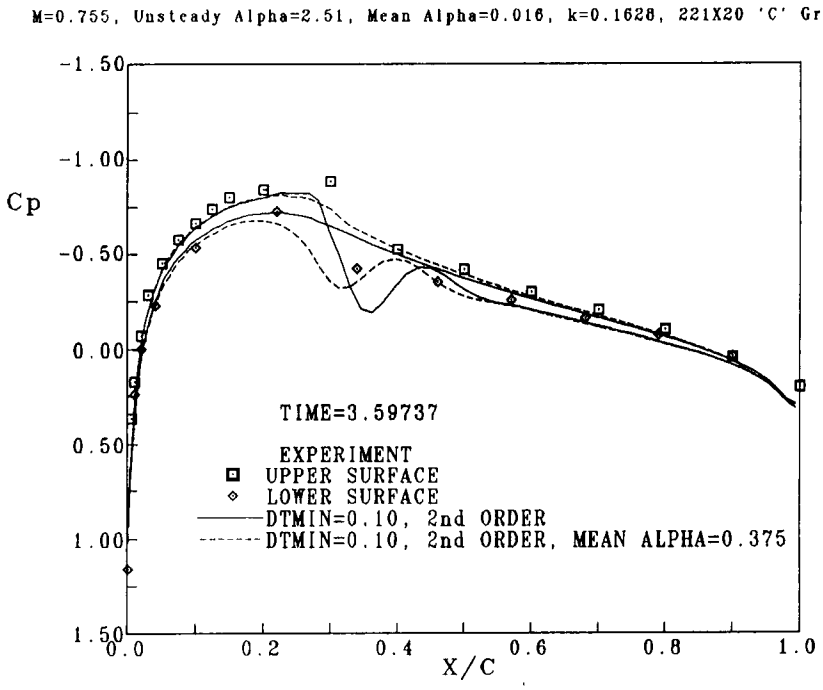

Figure 16

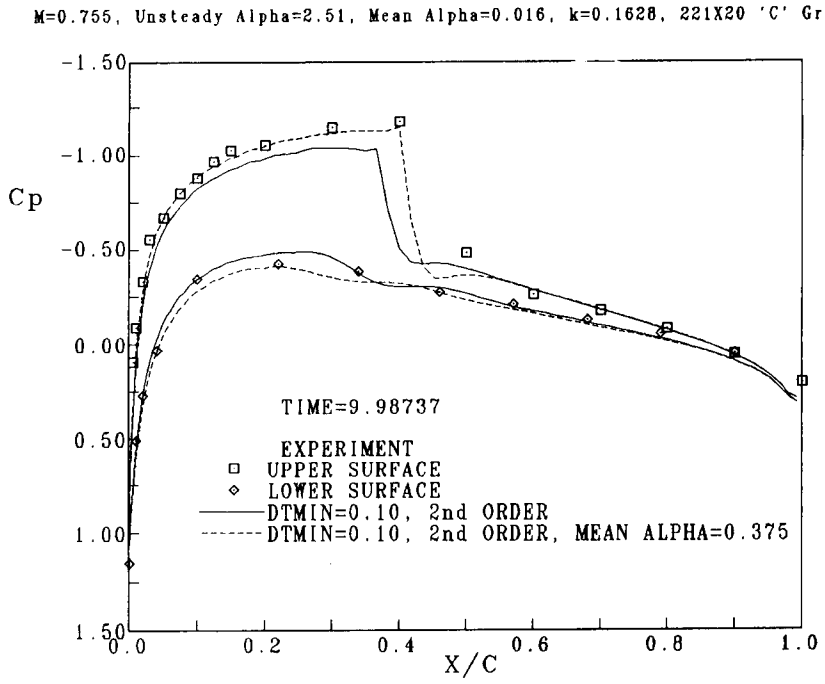

Figure 17

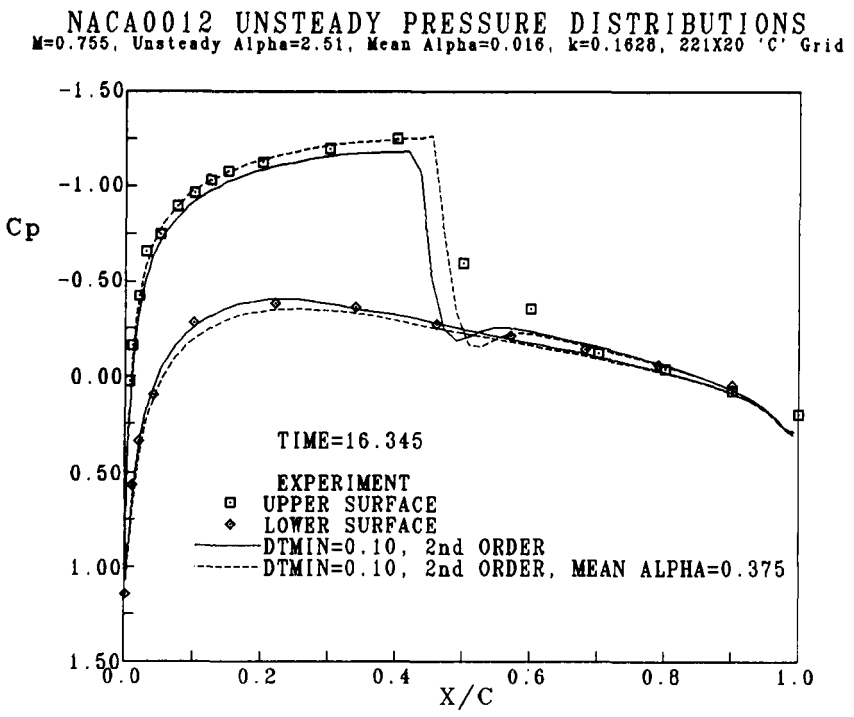

Figure 18

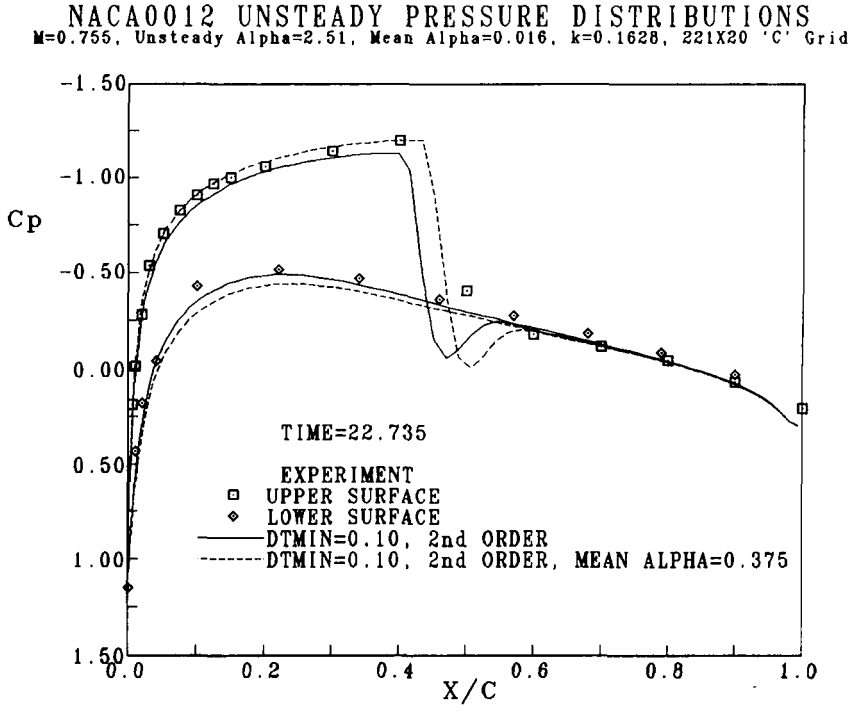

Figure 19

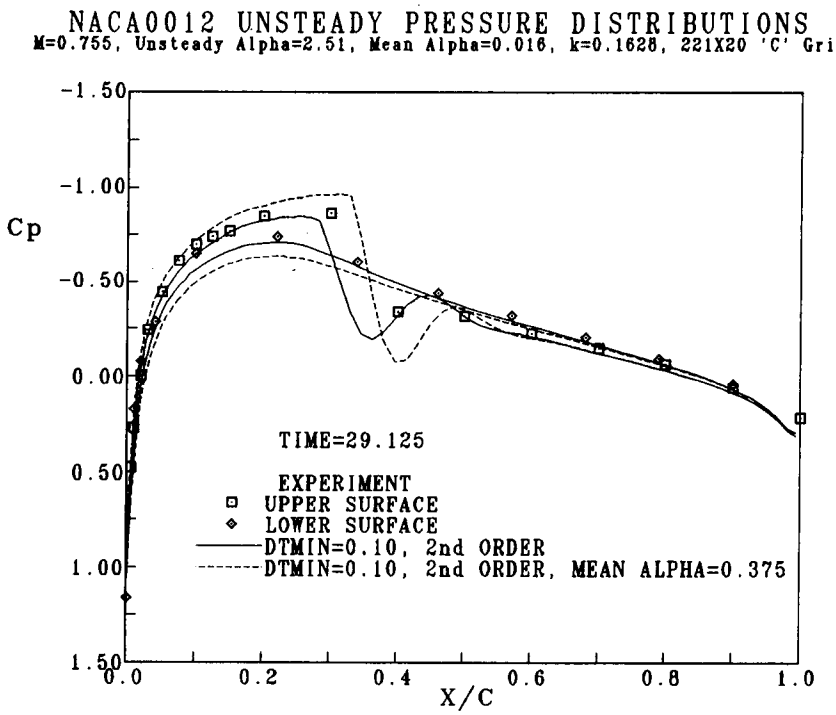

Figure 20

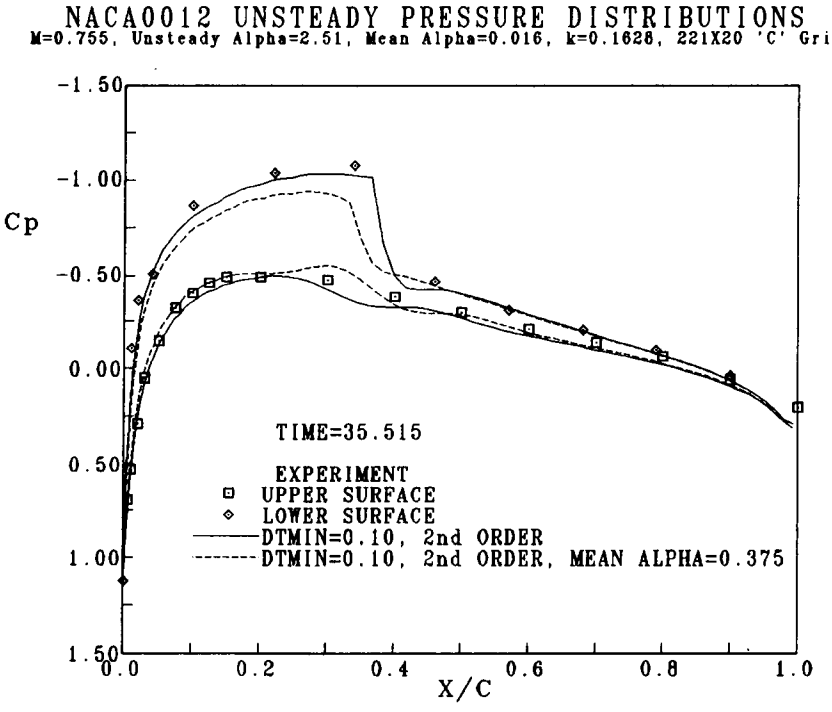

Figure 21

Rectangular Supercritical Wing

Euler calculations were performed to compare to the experimental results of Ricketts, et al (Reference 5). Calculations at a higher reduced frequency, k = 0.714, compare similarly to those presented here, k = 0.358. At higher Mach numbers, however, the comparison was much poorer due to mislocation of the shock by the inviscid Euler code. The time step size used resulted in 360 time steps per cycle of motion for the k = 0.358 case. Maximum Courant numbers near 500 occurred in the vicinity of the wing tip for this time step size. Fourier analysis of the third cycle of oscillation yielded the magnitude and phase of the unsteady pressures shown on subsequent figures. The three cycles of motion used 6357 seconds on a CRAY X-MP (Figure 22).

- EXPERIMENT BY RICKETTS, SANDFORD, WATSON, AND SEIDEL NASA TM 85765, AUG 84
- RECTANGULAR PLANFORM, ASPECT RATIO 4 (FULL SPAN)
- 12% THICK SUPERCRITICAL AIRFOIL
- OSCILLATORY PITCH ABOUT 46% CHORD
- CONDITIONS
  - MACH 0.70
  - 4 DEGREES MEAN ALPHA
  - ONE DEGREE UNSTEADY ALPHA
  - REDUCED FREQUENCY = 0.358 = $\frac{c\omega}{V_\infty}$

Figure 22

Rectangular Wing Blocked Grid

The wing calculations were carried out on a grid broken into four blocks to obtain the solution using only 2.6 million words of memory. The entire grid has dimensions 101x25x27. Block I contains all points below the wing, Block II contains points wrapping around the wing tip, Block III contains all points above the wing, and Block IV contains all points downstream of the wing (Figure 23). The method used to obtain time-accurate solutions on blocked grids is described in Reference 6. Motion of the wing is modelled by pitching the entire grid containing the wing as a rigid body using the time-dependent coordinate transformation described earlier.

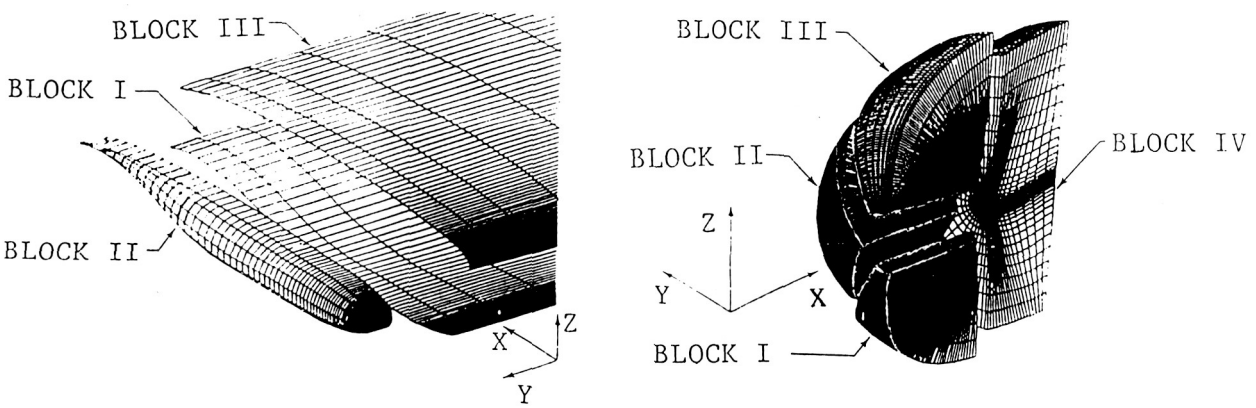

Figure 23

Rectangular Wing Pressures
at 60% Semispan

Steady pressures compare fairly well. There is a slight overshoot at the leading edge and the captured shock is aft of the experimental location (Figure 24). Unsteady pressure magnitude compares well except that the shock spike is downstream of the experimental location. Unsteady pressure phase calculations show excellent agreement up to the highly cambered trailing edge where the experiment and calculation differ slightly (Figures 25 and 26).

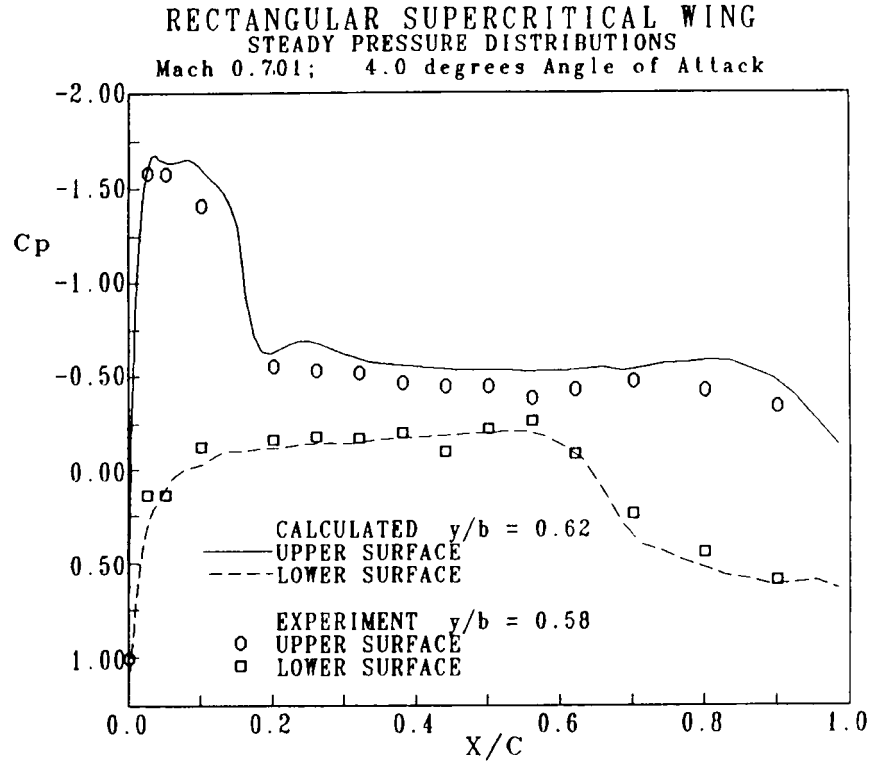

STEADY PRESSURE AT 60% SEMISPAN

Figure 24

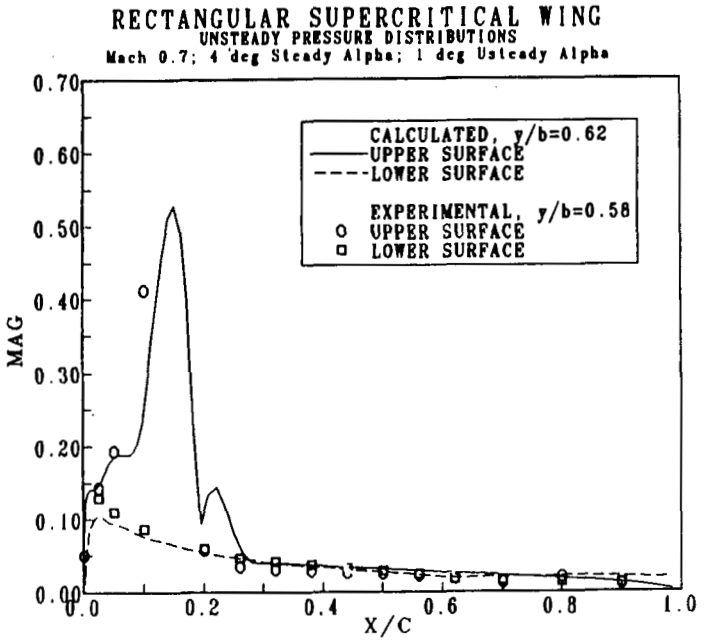

MAGNITUDE AT 60% SEMISPAN

Figure 25

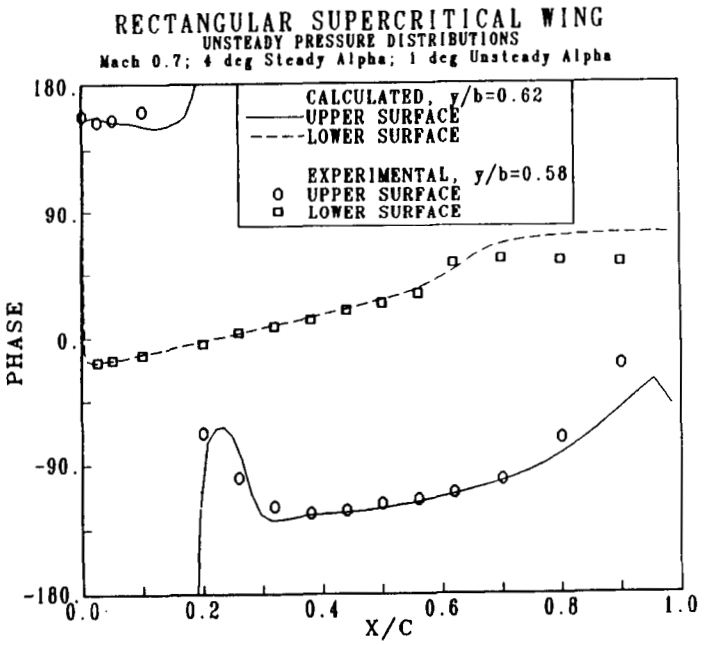

PHASE AT 60% SEMISPAN

Figure 26

Rectangular Wing Pressures at 95% Semispan

Steady pressures shown in Figure 27 underexpand slightly in the leading edge region but follow the experimental results very closely thereafter. The peak in unsteady pressure magnitude shown in Figure 28 near the leading edge is likewise calculated to be smaller than experiment. Phase results shown in Figure 29 are in excellent agreement.

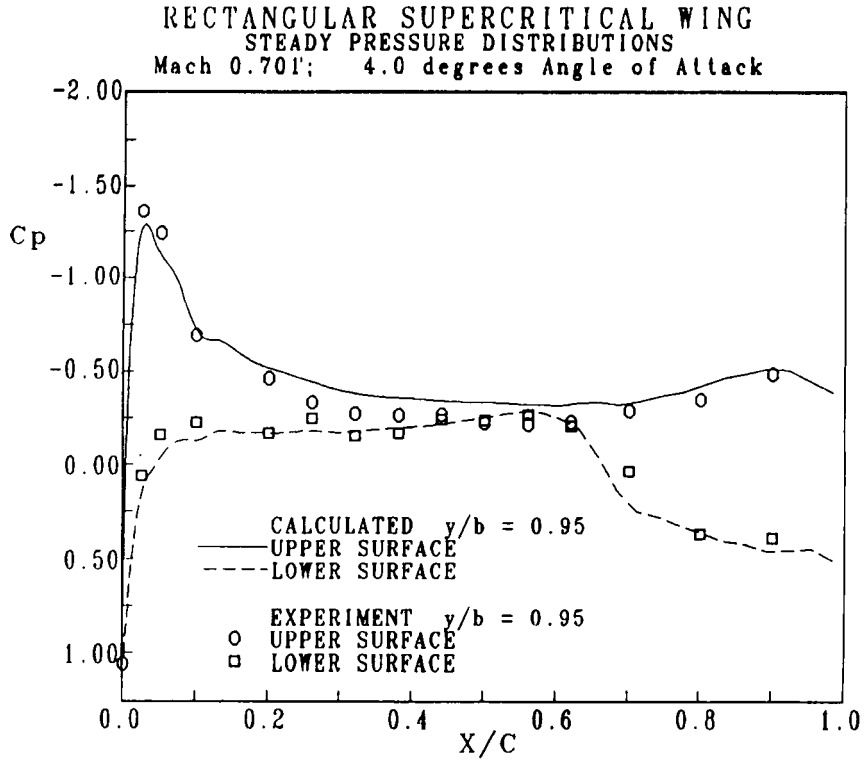

STEADY PRESSURE AT 95% SEMISPAN

Figure 27

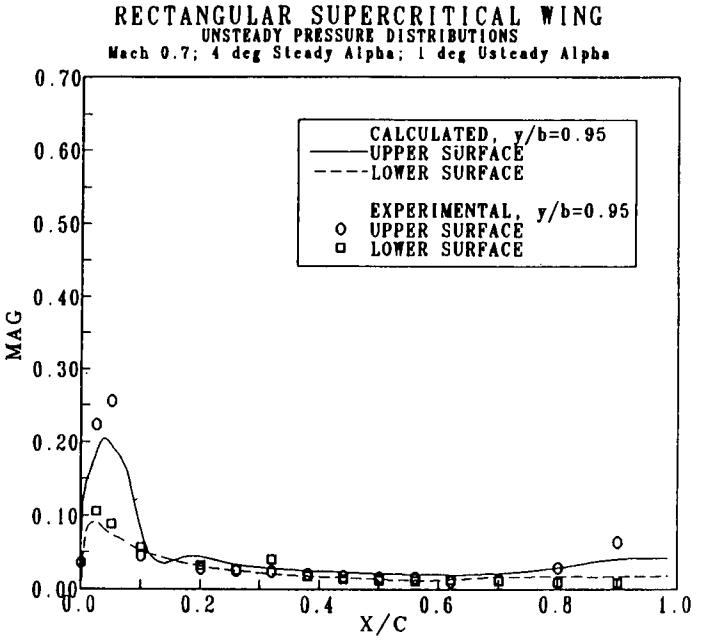

MAGNITUDE AT 95% SEMISPAN

Figure 28

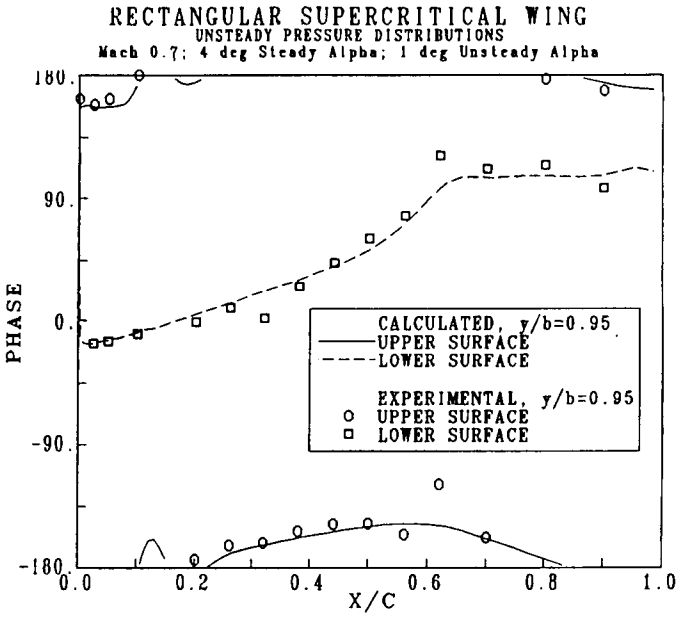

PHASE AT 95% SEMISPAN

Figure 29

CONCLUSIONS

- TIME-ACCURACY CAN BE OBTAINED AT COURANT NUMBERS MUCH GREATER THAN ONE
- FOR THE CASE PRESENTED, FREEZING FLUX JACOBIANS HAD LITTLE EFFECT ON TIME-ACCURACY
- EULER CALCULATIONS COMPARE WELL WITH NACA0012 AND SUPERCRITICAL WING EXPERIMENT
- VISCOSITY REQUIRED TO ACCURATELY MODEL SUPERCRITICAL WING

Figure 30

List of References

1. Belk, D.M., "Unsteady Three-Dimensional Euler Equations on Dynamic Blocked Grids," Dissertation, Mississippi State University, August 1986, available as AFATL-TR-86-74, October 1986.

2. Whitfield, D.L., "Implicit Upward Finite Volume Scheme for the Three-Dimensional Euler Equations," MSSU-EIRS-ASE-85-1.

3. Thompson, J.F., "A Composite Grid Generation Code for General Three-Dimensional Regions," AIAA Paper 87-0275, January 1987.

4. Landon, R.H., "NACA0012. Oscillatory and Transient Pitching," Compendium of Unsteady Aerodynamic Measurements, AGARD-R-702, August 1982.

5. Ricketts, R.H., Sandford, M.C., Watson, J.J., and Seidel, D.A., "Subsonic and Transonic Unsteady- and Steady-Pressure Measurements on a Rectangular Supercritical Wing Oscillated in Pitch," NASATM85765, August 1984.

6. Belk, D.M. and Whitfield, D.L., "Time-Accurate Euler Equations Solutions on Dynamic Blocked Grids," AIAA-87-1127-CP, AIAA 8th Computational Fluid Dynamics Conference, Honolulu, Hawaii, June 9-11, 1987.